Int. J. Electrochem. Sci., 14 **(2019)** 9404 – 9414, doi: 10.20964/2019.10.32

International Journal of
ELECTROCHEMICAL
SCIENCE
www.electrochemsci.org

Three-Dimensional Holey-graphene for Simultaneous Sensing in Biological Fluids

Aihua Jing[1], *Qiong Xu*[1], *Wenpo Feng*[1] *and Gaofeng Liang*[2,*]

[1] School of Medical Technology and Engineering, Henan University of Science and Technology, Luoyang 471023, P. R. China
[2] Medical college, Henan University of Science and Technology, Luoyang 471023, P. R. China;
[*]E-mail: lgfeng990448@haust.edu.cn

Received: 2 July 2019 / *Accepted:* 13 August 2019 / *Published:* 30 August 2019

The quantification of ascorbic acid (AA), dopamine (DA), uric acid (UA) and tryptophan (Trp) has been an important area of research, as these molecules directly correspond to diagnosing and controlling diseases related to nerve and brain physiology. In our research, novel sensors of three-dimensional holey-graphene (3DHGO) were fabricated from holey graphene oxide with nano pores via a reduction method, and their morphology, structure and electrochemical performance were characterized with X-ray diffraction, Fourier transform infrared spectroscopy, scanning electron microscopy, transmission electron microscopy and cyclic voltammograms. The proposed 3DHGO displayed excellent electron transport properties, high sensitivity and selectivity for the simultaneously detection of AA, DA, UA and Trp in healthy human serum and urine samples. This finding paves the way for the application of graphene as a biosensor for medical diagnosis.

Keywords: Three dimensional; Holey graphene; Electrochemical biosensor; Simultaneous detection

1. INTRODUCTION

Electrochemical biosensors are good at detecting several compounds in pharmaceutical and biological samples.[1-3] However, the detection is sometimes limited by selectivity due to interference from species with similar electroactive potentials. Three-dimensional (3D) graphene architectures have been widely used in electrochemical capacitors, [4, 5] electro catalysts, [6] biosensors [7] and lithium-ion batteries [8]. Its superior electrical properties and biocompatibility make it an ideal material in electrochemical sensors applications. [9] In this context, various 3D graphene structures such as graphene oxide foams loaded with AuPd alloy, [10] Au nanoparticles/nano-poly(3,4-ethylene dioxythiophene)-graphene aerogel [11] and three-dimensional-graphene with hydroxypropyl--cyclodextrin [12] have been explored in electroanalysis in order to improve the sensitivity, selectivity

and stability of the electrode. Most of the above-mentioned 3D graphene sensors were graphene composites prepared by 3D graphene that was then mixed with oxide, an elementary substance or organic materials. Therefore, it is still of great interest and importance to develop new 3D graphene materials with high specific surface areas and designed porosities.

The human body is primarily composed of fluid as the internal environment, and it contains a large amount of electrolytes, including inorganic and organic electrolytes.[13] Small biomolecules such as L-ascorbic acid (AA), uric acid (UA), dopamine (DA) and tryptophan (Trp), which play important roles in human metabolism, can be found in body fluids. AA is a water-soluble vitamin and one of the essential nutrients of the body. It plays a regulatory role in the treatment of scurvy and cancer.[14] High uric acid levels are the result of an imbalance in the metabolism of uric acid in the blood. Excessive uric acid can cause gout, hyperuricaemia, coronary heart disease, diabetes and kidney stones.[15, 16] DA is an important neurotransmitter in the brain. It plays an important role in shock syndrome and cardiovascular disease, Parkinson's disease and neuroendocrine disorders caused by infarction and renal failure.[17, 18] Trp is an essential amino acid that plays an important role in the treatment of insomnia, liver function decline, and tryptophanuria.[19] AA, DA, UA and Trp usually coexist in body fluids, but their oxidation potentials at common solid electrodes are similar. Moreover, it is necessary to detect them simultaneously in attempts to understand the mechanism of biomedical and diagnostic pathology. Therefore, the development of sensors simultaneously sensitive to and selective for AA, DA, UA and Trp is very important for the study of physiological functions as well as diagnostic and analytical applications. In recent years, various materials such as hemin-graphene oxide-pristine carbon nanotubes complexes, [20] iron ion-doped natrolite zeolite-multiwalled carbon nanotubes, [19] multi-walled carbon nanotube/Azure A/gold nanoparticle composites, [21] multi-walled carbon nanotubes (MWNTs) bridged mesocellular graphene foam (MGF) nanocomposite, [22] silver nanoparticles-decorated reduced graphene oxide, [23] and graphene hybrid tube-like structures [24] have been used to modify conventional electrodes due to their remarkable electrocatalytic properties for the simultaneous detection of AA, DA, UA and Trp. Among these materials, carbon nanotubes and its composite film are attractive electrochemical sensors and biosensors due to their excellent electron transfer rate and high surface area. Novel materials of graphene or its composite are expected to show high potential for developing new electrode material to simultaneously detect AA, DA, UA and Trp.

Here, we report a facile preparation of holey graphene oxide (HGO) with nano-pores via a convenient mild defect-etching reaction. A biosensor of 3DHGO with large specific surface area was successfully fabricated by a reduction induced self-assembly method. A graphic illustration of the fabrication and detection strategy is displayed in Scheme 1. The 3DHGO/GCE was further used in electrochemical determination of AA, DA, UA and Trp simultaneously by differential pulse voltammetry, showing an ultra-low detection limit, high sensitivity and good repeatability. In addition, the mechanism of the 3DHGO ability to simultaneous detect multiple biomolecules was evaluated. The achieved satisfactory recoveries in healthy human serum and urine samples indicated the practical application potential of the sensor and further opened a new avenue for electrochemical biosensors of graphene-based advanced materials in new fields of medical diagnosis.

2. EXPERIMENTAL

2.1. Materials and Apparatus

Graphite powder prepared in our lab was made a 0.1 mg mL^{-1} solution. AA was purchased from Tianjin Fengchuan Chemical Reagent Technology Co., Ltd. (Tianjin). Both UA and Trp were purchased from Shanghai Sangon Bioengineering Co., Ltd. (Shanghai). DA was purchased from Shanghai Maclean Biochemical Co., Ltd. (Shanghai). All other reagents were of analytical grade and used without any purification process. Phosphate buffer solution (PBS) were prepared by using a mixed solution of 0.1 M Na_2HPO_4 and 0.1 M NaH_2PO_4, followed by adjusted with 100 mM NaOH or H_3PO_4. Twice-distilled water was used to prepare all solutions.

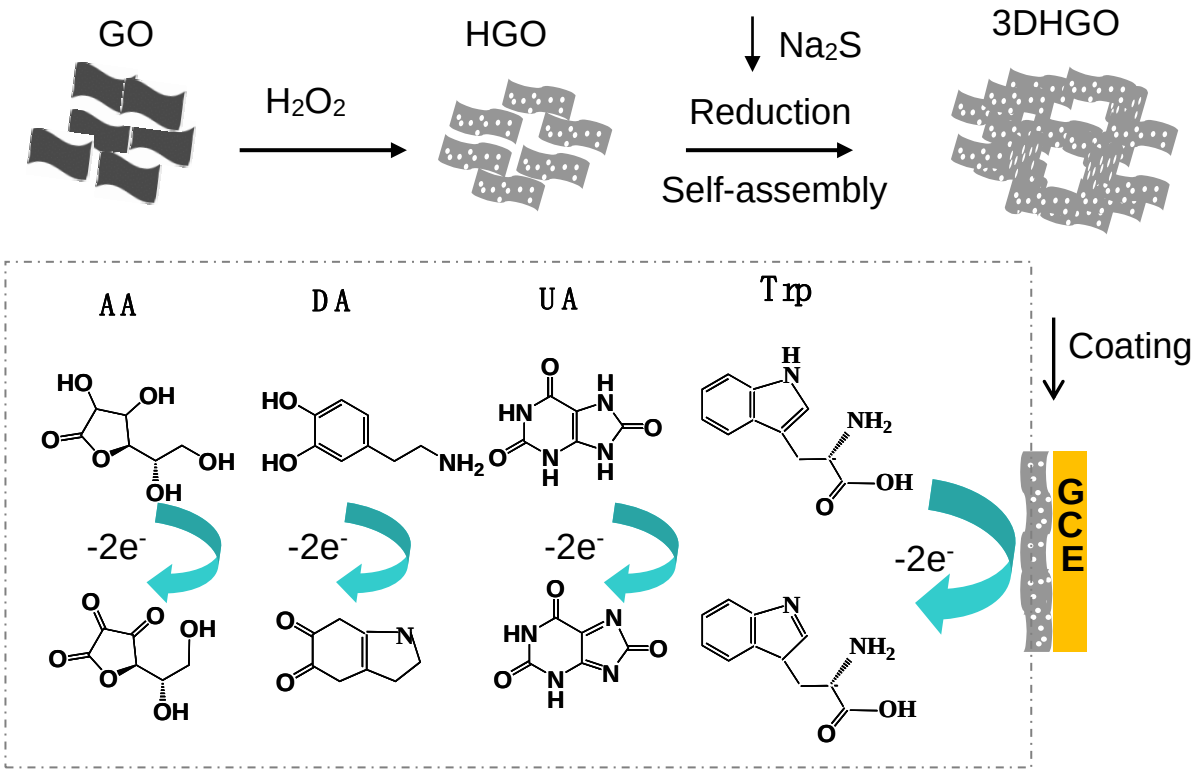

Scheme 1. A scheme for the preparation of three-dimensional (3D) holey-graphene oxide (3DHGO)/glass carbon electrode (GCE) biosensor and the reaction mechanism of AA, DA, UA and Trp on it.

Data acquisition was performed at room temperature using a Nicolet 6700 Fourier transform infrared (FTIR) spectrum manufactured by Thermo Fisher, USA, with a spectral range of 400 to 4000 cm^{-1}. A JEOL JSM IT100 scanning electron microscope (SEM) and a JEOL JTM-2100 transmission electron microscope (TEM) were used to character the morphologies of the product. A D8 ADVANCE X-ray diffractometer was used to acquir the X-ray diffraction (XRD) measurements. All electrochemical measurements were performed on a CHI660E workstation (Chenhua Instruments, Shanghai, China) with a three-electrode system. 3DHGO/GCE or HGO/GCE was used as the working electrode. Solutions were degassed with nitrogen to remove O_2.

2.2. Preparation of holey graphene oxide (HGO)

Graphene oxide (GO) was prepared from purified natural graphite according to a modified Hummers' method.[25, 26] To prepare HGO, 5 mL of 30% H_2O_2 solution was mixed with 50 mL of GO solution, and the mixed product was uniformly heated and stirred for 4 h at 100 °C. The as-prepared HGO was purified by centrifuging followed by washing with pure water to remove the residuals and finally re-dispersed in pure water to produce a 2 mg mL^{-1} HGO solution of. [27, 28]

2.3. Preparation of 3DHGO

Na_2S (0.034 g) was dissolved in 80 mL of an HGO aqueous suspension (0.2 mg mL^{-1}) and stirred for 10 min at 0 °C. Diluted HCl aqueous solution (5 mL, 0.024 M) was added dropwise into the above solution with stirring. After reacting for 10 h, the obtained product was collected and washed with deionized water. After being re-dispersed into 28 mL deionized water, 2.8 mL of a sodium ascorbate ($C_6H_7O_6Na$) aqueous solution (1 M) was added in ultrasonically and then heated at 95 °C for 1.5 h. The product was washed with deionized water to remove any impurities, resulting in 3DHGO can be obtained.[29]

2.4. Electrochemical studies

A glass carbon electrode (GCE) was first polished to a mirror with 0.3 and 0.05 μm alumina slurry (Beuhler) then sonicated in acetone, nitric acid solution (1:1, V/V) and pure water. The electrode was kept at 4 °C for a day after 20 μL of 2.0 mg mL^{-1} 3DHGO was cast evenly on the treated surface of the GCE (diameter: 3 mm) and dried at room temperature. Five microliters of a 0.5% Nafion solution were then dropped cover the surface. Differential pulse voltammograms (DPVs) were recorded at 0.1 M PBS (pH 7.0) at different concentrations of AA, DA, UA and Trp. For real sample detection, human serum samples and urine samples were diluted with 0.1 M PBS (pH 7.0) before electrochemical determination and then transferred to the electrochemical cell.

3. RESULTS AND DISCUSSION

3.1. Structures and Morphologies of 3DHGO

Figure 1a displays SEM images of 3DHGO. Graphene sheets are interconnected and stacked together forming three-dimensional structure. The as-prepared 3DHGO samples possess interlinked porous networks. And caves with sizes of submicrometers to several micrometers could be seen. The porous networks structures will enable electron fast and mass transport in electrochemical researches. TEM image (Figure 1b) reveals another porous structure of 3DHGO that pores of several nanometers decorated on the sheets of HGO, which is the complementarity of the further exquisite structures of the SEM images.

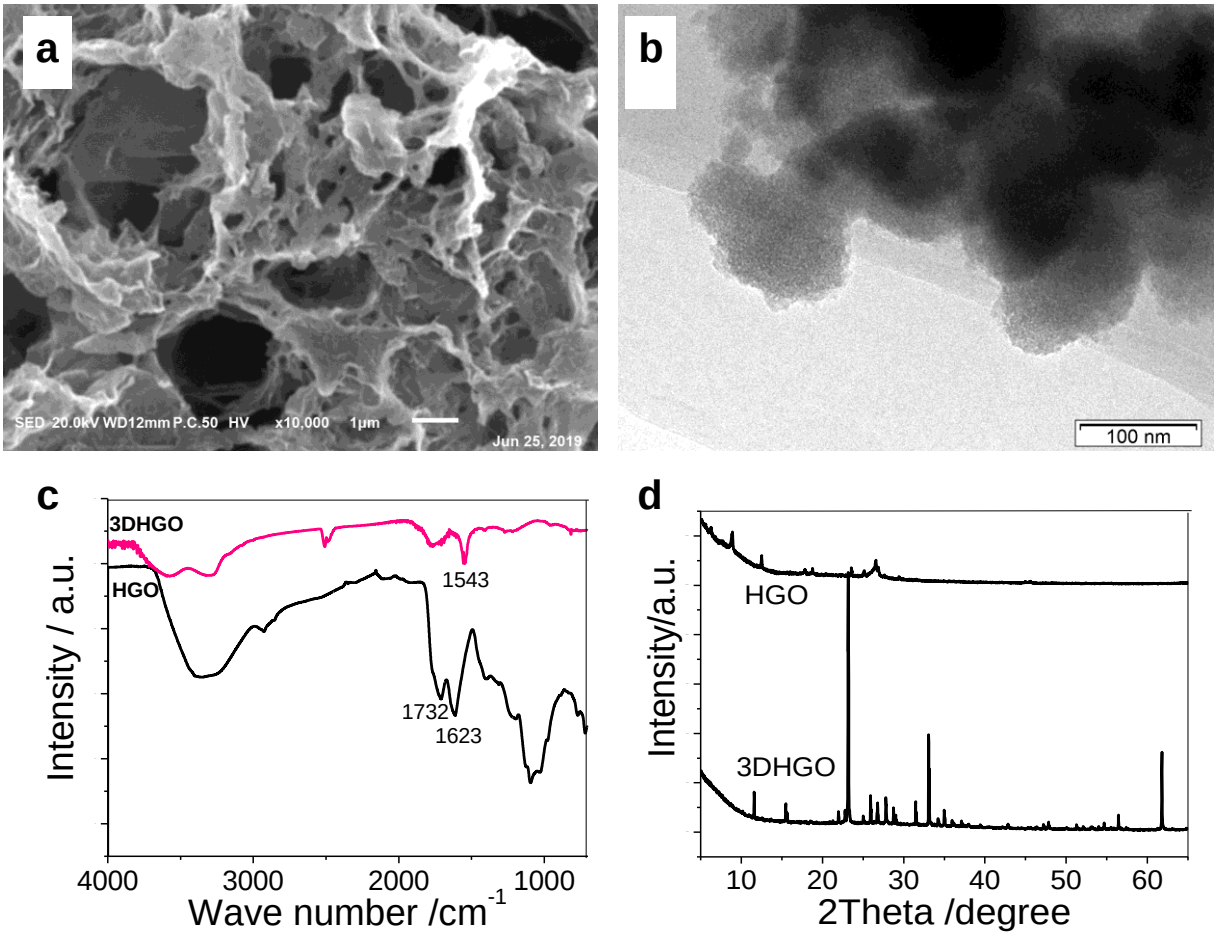

Figure 1. The SEM image (a) and TEM image (b) of three-dimensional holey graphene. FT-IR spectrum (c) and XRD pattern (d) of three-dimensional holey graphene and holey graphene.

Figure 1c shows FT-IR spectrum of 3DHGO and HGO. Compared 3DHGO with HGO, three peaks at 1732, 1623 and 1053 cm^{-1} are found greatly weakened. These peaks are ascribed to C═O bonds, carboxyl O═C–O and C–O bonds, there weakening indicated that the GO has been reduced. [30, 31] A new peak presents at 1543 cm^{-1} in the spectra of 3DHGO ascribe to the stretching vibrations of S–O. [31, 32] The S–O bonds could effect immobilize the polysulfides.[29]

Figure 1d shows the XRD diffraction characteristics of 3DHGO and HGO. Compared to HGO, 3DHGO composites have three high-strong diffraction peaks. From the overall trend of the diffraction peaks, high and sharp peaks are seen, which proves that the prepared sample has relatively large crystal grains, good crystallinity, and the structure of the microcrystal layer is orderly in spatial layout. The difference of the XRD patterns between 3DHGO and HGO demonstrates that the heterogeneous nucleation of sulfur may have been facilitated by the graphene oxide solution because of the abundant of functional groups on the graphene oxide nanosheets surface.[29, 33]

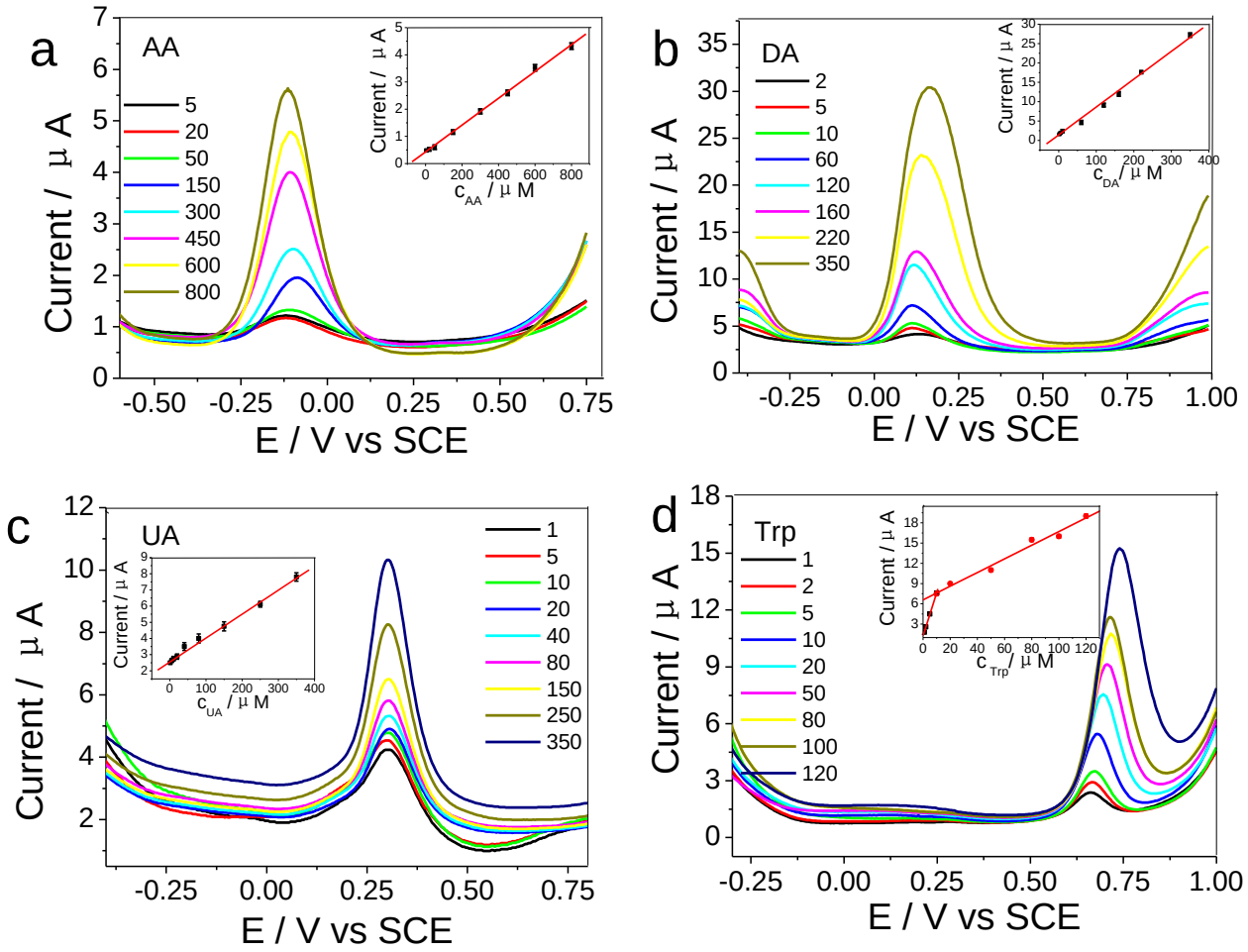

Figure 2. DPVs of 3DHGO/GCE under increasing concentrations of AA (a), DA (c), UA(c) and Trp (d). Inset: The plots of oxidation peak currents versus concentration of each biomolecules.

3.2. 3DHGO for Electrochemical Determination of AA, DA, UA and Trp

The detection of AA, DA, UA and Trp individually was carried out in PBS solution. Figure 2 shows the DPV and calibration curves obtained under 3DHGO/GCE with increased concentrations of AA(a), DA(b), UA(c) and Trp (d). Four distinct oxidation potentials were observed from lowest to highest: AA (−0.107 V) < DA (0.103 V) < UA (0.29 V) < Trp (0.65 V). With increased of the concentration, the oxidation current increased linearly accordingly. In the range of 5~800 μM, the peak current density of AA is directly proportional to the concentration with the linear regression equation of Δj (mA·cm^{-2}) = 4.942 × 10^{-3} + 0.04328 c (μM) (R^2=0.9991). In the range of 2~350 μM, the peak current density of DA is directly proportional to the concentration with the linear regression equation of Δj (mA·cm^{-2}) = 7.184×10^{-3} + 0.1436 c (μM) (R^2=0.9982). In the range of 1~350 μM, the peak current density is directly proportional to the UA concentration with the linear regression equation of Δj (mA·cm^{-2}) = 1.471×10^{-3} + 0.2545 c (μM) (R^2=0.9968). In the range of 1~120 μM, the peak current density is directly proportional to Trp concentration with a linear regression equation of Δj (mA·cm^{-2}) = 4.6307 × 10^{-3} + 0.0467 c (μM) (R^2=0.9543). The detection limits (S/N=3) for AA, DA, UA, and Trp

are 1 μM, 0.5 μM, 0.2 μM, and 0.5 μM, respectively, which were slightly lower than the previously reported detection limits of the carbon-based nanomaterial-modified electrode. Evidently, the excellent low detection limit and high sensitivity of 3DHGO modified electrode can achieve the determination of small biomolecules in practical applications. This electrode will show the concentration of the substance to be analysed in the diluted actual sample in a linear range.

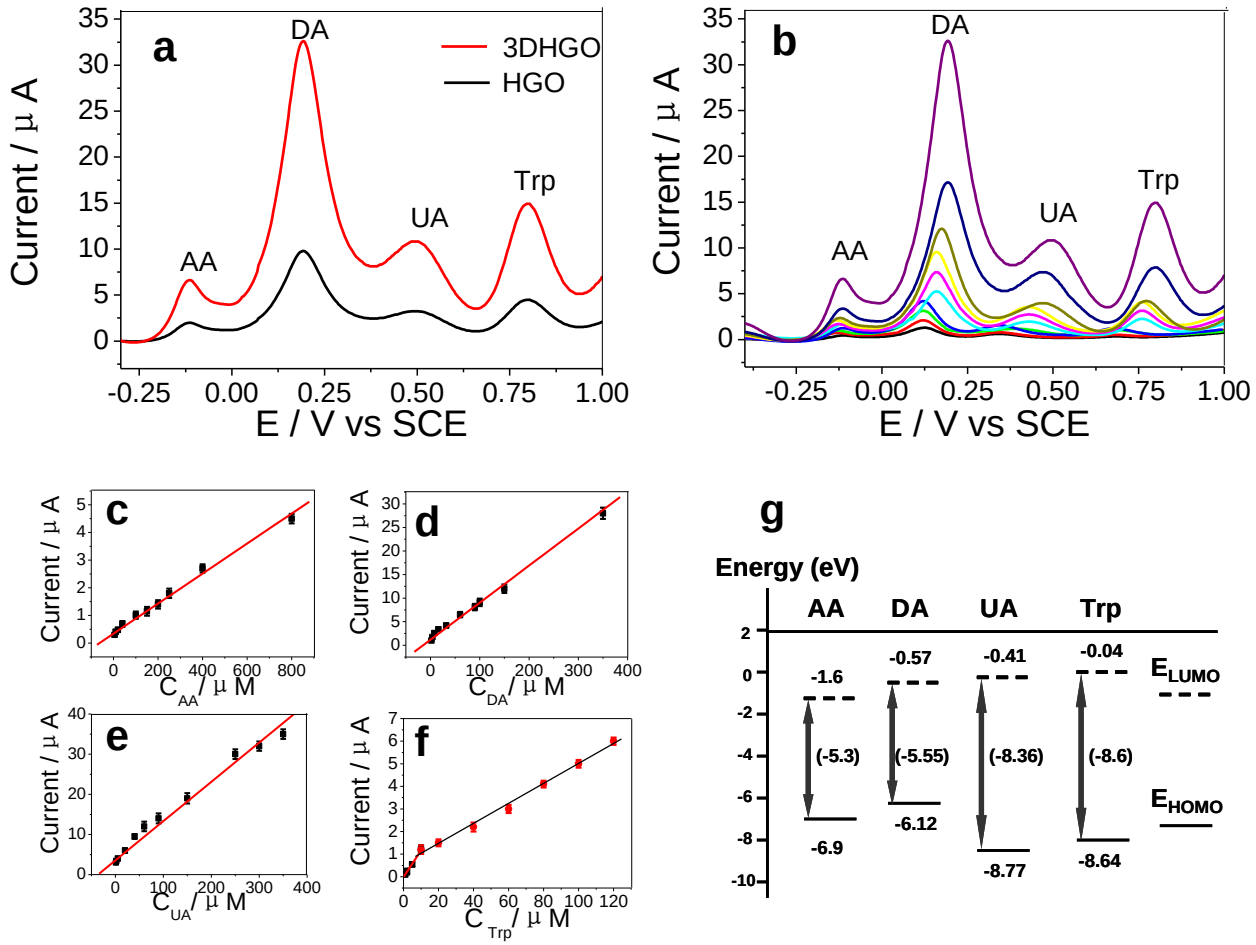

Figure 3. (a) DPVs at HGO/GCE and 3DHGO/GCE containing 800 μM AA, 300 μM DA, and 300 μM UA and 100 μM Trp. scan rate: 50 mV s^{-1}. (b) DPVs of 3DHGO/GCE for the simultaneous determination of AA, DA, UA and Trp in 0.1 M PBS solution. Calibration curves of 3DHGO/GCE for simultaneous determination of (c) AA, (d) DA, UA (e) and Trp (f). (g) Frontier molecular orbitals of AA, DA, UA and Trp.

The oxidation potential is generally controlled by electron transfer from the biomolecules to the 3D HGO electrode and hole transfer from the biomolecules to the counter electrode. The oxidation potential is determined by the highest occupied molecular orbital (HOMO) of biomolecules, and energy gaps between the HOMO and lowest unoccupied molecular orbital (LUMO) of the biomolecules on the electrode. AA, DA, UA and Trp moleculars orbital analyses of the HOMO and the LUMO are listed in Figure 3g. The LUMO-HOMO energy gaps were, from lowest to highest, AA (5.3 eV) ‹ DA (5.55 eV) ‹ UA (8.36 eV) ‹ Trp (8.6 eV). The oxidation potential decreases with the

decrease in the LUMO-HOMO energy gap, which agrees with our results in Figure 2 and Figure 3a.[34]

The reaction mechanism of sensing between biomolecules of AA, DA, UA, Trp and 3DHGO/GCE is shown in Scheme 1. The anodic peaks observed on the electrode corresponding to the oxidation of hydroxyl groups of the furan ring in AA changed to carbonyl groups, the oxidation of catechol in DA changed to o-quinone, the oxidation of bridging double bonds in UA changed to hydroxyl groups, and the oxidation of the phenyl ring in Trp. Moreover, two protons and two electrons were participated in the oxidation processes. Graphene nanosheets can be adsorbed strongly with aromatic rings because firm π-π interactions between the free π-bonds of sp^2 atoms of the six-benzene-ring graphene and the aromatic rings. The oxidation peak current is determined by the adsorption affinities. There are aromatic rings in DA, UA and Trp molecular structures, leading to strong adsorption; thus, high oxidation peaks of currents were obtained which result in higher sensitivity in detecting of DA, UA, and Trp than AA. [35]

The simultaneous detecting of AA, DA, UA and Trp was carried out in PBS buffer solutions. Figure 3a exhibits DPVs of 3DHGO/GCE and HGO/GCE in 0.1 M PBS including 800 μM AA, 300 μM DA, 300 μM UA and 100 μM Trp. For the 3DHGO/GCE, four separated anodic peaks were discovered at -0.107, 0.210, 0.492, and 0.685 V, in accordance with the electro-oxidation of AA, DA, UA and Trp, separately. There are 0.317 V potential differences between the anodic peak of AA and DA, 0.282 V between DA and UA, and 0.193 V between UA and Trp. Moreover, the oxidation current densities for these four biomolecules at 3DHGO/GCE were much higher than those at HGO/GCE. The results demonstrated that 3DHGO/GCE possesses excellent electrocatalytic activity for the oxidation of AA, DA, UA and Trp biomolecules. This result could probably be attributing to the distinctive highly porous 3D structure with great electrochemically active surface areas, which facilitated the rapid and quick electron transport between the biomolecules and the electrode surface.

The linear range obtained by simultaneously measuring these four biomolecules is the same as that obtained by the respective detections, and the slopes are equivalent (Figure 3b-e), indicating that protons were involved in their electrode reaction processes and that the 3DHGO is exposed to many edge defects and active sites from edge defects. The proposed method was compared with other electrochemical methods in the literature listed in Table 1. The 3DHGO/GCE displayed a linear range and a detection limit for AA, DA, UA and Trp that is similar to most of the electrodes listed below.

The 3DHGO/GCE electrodes were placed into 0.1 M PBS buffers and a mix of 650 μM AA, 300 μM DA, 200 μM UA and 75 μM Trp. The relative standard deviations of three consecutive measurements for AA, DA, UA and Trp were 3.2%, 4.7%, 2.9% and 4.3%, respectively. In addition, 3DHGO/GCE was placed in 0.1 M PBS and stored at 0 °C for 14 days without showing significant current response attenuation, indicating that the prepared 3DHGO/GCE electrode has good stability. To evaluate the influence of various interference on the detecting ability of 3DHGO/GCE electrode, several biological, organic and inorganic compounds were selected to add into the detected mixture for interference tests. The results showed that when 650 μM AA, 300 μM DA, 200 μM UA and 75 μM Trp were simultaneously detected, citric acid, glucose, L-cysteine, L-glycine, L-lysine, L-tyrosine, aniline, phenol were added individually (the concentrations of each were 200 μM).

Table 1. Comparison of other carbon-based materials for the simultaneous determination of AA, DA, UA and Trp.

Electrode	Detection limit (μM) (Linear range (μM))				Ref.
	AA	DA	UA	Trp	
Iron /natrolite zeolite /multiwalled carbon nanotube	1.11 (7.77-833)	1.05 (7.35-833)	0.033 (0.23-83.3)	0.011 (0.074-34.5)	[17]
Hemin/graphene oxide/carbon nanotubes	0.17 (0.5-2.16)	0.017 (0.05-2.65)	0.017 (0.05-1.49)	0.017 (0.05-2.65)	[18]
multi-walled carbon nanotube/Azure A/gold	16 (300-10000)	0.014 (0.5-50)	0.028 (0.5-50)	0.56 (1.0-100)	[19]
multi-walled carbon nanotubes/graphene foam	18.28 (100-6000)	0.06 (0.3-10)	0.93 (5-100/300-1000)	0.87 (5-30/60-500)	[20]
Ag nanoparticles/rGO/GCE	9.6 (10-800)	5.4 (10-800)	8.2 (10-800)	7.5 (10-800)	[21]
graphene hybrid tube-like structures	5.60 (20-400)	0.13 (0.40-374)	0.92 (4-544)	0.06 (0.4-138)	[22]
3DHGO/GCE	1.0 (5-800)	0.5 (2-350)	0.2 (1-350)	0.5 (1-120)	This work

Table 2. Determination of AA, DA, UA and Trp in samples using three-dimensional holey-graphene (n = 5).

Sample	Analyte	Detected(μ M) [a]	Added(μ M)	Found(μ M) [a]	Recovery(%)
Serum	AA	0	50	48.8±1.1	97.6
	DA	0	20	19.7±0.6	98.5
	UA	0	30	31.4±0.8	104.7
	Trp	0	40	39.2±0.7	98
Urine	AA	0	40	43.2±1.2	108
	DA	0	25	26.1±0.8	104.4
	UA	12.6±0.3	40	54.8±1.2	104.2
	Trp	0	30	29.7±1.1	99

[a] Mean±standard deviation for n = 5.

The peak potential and peak current of the four biomolecules are basically unchanged, showing little interference; when $CaCl_2$, KNO_3, Mg $(NO_3)_2$, Na_2SO_4, and NaCl were added individually (50 mM), the peaks were also basically unchanged, revealing no large interference. These results strongly demonstrated that the as-prepared 3DHGO/GCE electrode has high selectivity.

3.3. Real sample analysis

To evaluate the potential applicability of the sensor constructed by the 3DHGO/GCE, the 3DHGO/GCE electrode was used to detect AA, DA, UA and Trp in healthy human serum and urine samples using the standard adding method. The serum and urine samples were diluted 5 and 100 times respectively with 0.1 M PBS (pH 7.0) before the test. The electrochemical response of AA, DA, UA and Trp showed that the recoveries of all biomolecules were within the range of 97.6% and 108% (Table 2). These results demonstrated that 3DHGO/GCE is a good material for the accurate detection AA, DA, UA and Trp in clinical diagnosis, which is of significant value in the application of biological samples.

4. CONCLUSIONS

In this study, we constructed a simple system using 3DHGO/GCE as an electrochemical biosensor electrode, which not only can separate the oxidation peaks of AA, DA, UA and Trp, such that the four substances can be detected simultaneously, but also has the advantages of rapid reaction, high sensitivity and low detection limit. At the same time, the interference test and stability test also show that the electrode has the anti-interference ability and stability conditions required in practical applications. Finally, by measuring the recovery rate of human serum samples, the three-dimensional holey-graphene exhibits extremely high stability and is suitable for the detection of these four biomolecules in human serum for medical applications.

ACKNOWLEDGEMENTS

This work was financially supported by projects grant from the National Natural Science Foundation of China (U1404824 and 81741147), Henan International Cooperation in Science and Technology (172102410083), the Natural Science Foundation of Henan Province (182300410270) and Innovation Scientists and Technicians Troop Construction Projects of Henan Province.

References

1. W. Deng, X. Yuan, Y. Tan, M. Ma, Q. Xie, *Biosens. Bioelectron.*, 85 (2016) 618.
2. L.J. Xu, S.W. Xie, J.G. Du, N.Y. He, *Journal of Nanoscience and Nanotechnology*, 17 (2017) 238.
3. A.R. Taheri, A. Mohadesi, D. Afzali, H. Karimi-Maleh, H.M. Moghaddam, H. Zamani, Z.R. Zad, *International Journal of Electrochemical Science*, 6 (2011) 171.
4. H.Z. Wang, C. Shen, J. Liu, W.G. Zhang, S.W. Yao, *Journal of Alloys and Compounds*, 792 (2019) 122.
5. Z.Q. Wen, M. Li, S.J. Zhu, T. Wang, *International Journal of Electrochemical Science*, 11 (2016) 23.
6. Z.Q. Gao, M.M. Li, J.Y. Wang, J.X. Zhu, X.M. Zhao, H.J. Huang, J.F. Zhang, Y.P. Wu, Y.S. Fu, X. Wang, *Carbon*, 139 (2018) 369.
7. M. Mazaheri, H. Aashuri, A. Simchi, *Sensors and Actuators B-Chemical*, 251 (2017) 462.
8. Y.F. Li, Y.Y. Fu, S.H. Chen, Z.Z. Huang, L. Wang, Y.H. Song, *Composites Part B-Engineering*, 171 (2019) 130.
9. P. Yu, R.Y. Bao, X.J. Shi, W. Yang, M.B. Yang, *Carbohydrate Polymers*, 155 (2017) 507.
10. Y.B. Hou, K. Sheng, Y. Lu, C. Ma, W. Liu, X.J. Men, L. Xu, S.Y. Yin, B. Dong, X. Bai, H.W. Song, *Microchimica Acta*, 185 (2018)397.
11. H.Y. Jia, J.K. Xu, L.M. Lu, Y.F. Yu, Y.X. Zuo, Q.Y. Tian, P. Li, *Sensors and Actuators B-Chemical*,

260 (2018) 990.
12. W. Liang, Y. Rong, L. Fan, W.J. Dong, Q.C. Dong, C. Yang, Z.H. Zhong, C. Dong, S.M. Shuang, W.Y. Wong, *Journal of Materials Chemistry* C, 6 (2018)12822.
13. G. Liang, S. Kan, Y. Zhu, S. Feng, W. Feng, S. Gao, *International Journal of Nanomedicine*, 13 (2018) 585.
14. X. Wei, Y. Xu, F.F. Xu, L. Chaiswing, D. Schnell, T. Noel, C. Wang, J. Chen, D.K. St Clair, W.H. St Clair, *Cancer Research*, 77 (2017) 1345.
15. X. Lian, B. Yan, *Inorganic Chemistry*, 56 (2017) 6802.
16. S. Biscaglia, C. Ceconi, M. Malagù, R. Pavasini, R. Ferrari, *International Journal of Cardiology*, 213 (2016) 28.
17. N.D. Volkow, R.A. Wise, R. Baler, *Nature Reviews Neuroscience*, 18 (2017) 741.
18. F.A. Zucca, J. Segura-Aguilar, E. Ferrari, P. Muñoz, I. Paris, D. Sulzer, T. Sarna, L. Casella, L. Zecca, *Progress in Neurobiology*, 155 (2017) 96.
19. M. Noroozifar, M. Khorasani-Motlagh, R. Akbari, M.B. Parizi, *Biosens. Bioelectron.*, 28 (2011) 56.
20. Y. Zhang, Z. Xia, H. Liu, M.J. Yang, L.L. Lin, Q.Z. Li, *Sensors and Actuators B-Chemical*, 188 (2013) 496.
21. H. Filik, A.A. Avan, S. Aydar, *Arabian Journal of Chemistry*, 9 (2016) 471.
22. H.X. Li, Y. Wang, D.X. Ye, J. Luo, B.Q. Su, S. Zhang, J.L. Kong, *Talanta*, 127 (2014) 255.
23. B. Kaur, T. Pandiyan, B. Satpati, R. Srivastava, *Colloids and Surfaces B-Biointerfaces*, 111 (2013) 97.
24. W. Zhang, Y.Q. Chai, R. Yuan, S.H. Chen, J. Han, D.H. Yuan, *Anal. Chim. Acta*, 756 (2012) 7.
25. W.L. Song, X.T. Guan, L.Z. Fan, Y.B. Zhao, W.Q. Cao, C.Y. Wang, M.S. Cao, *Carbon*, 100 (2016) 109.
26. H.M. Jin, S.H. Lee, J.Y. Kim, S.W. Son, B.H. Kim, H.K. Lee, J.H. Mun, S.K. Cha, J.S. Kim, P.F. Nealey, *Acs Nano*, 10 (2016) 3435.
27. N. Islam, S. Li, G. Ren, Y. Zu, J. Warzywoda, W. Shu, Z. Fan, *Nano Energy*, 40 (2017) 107.
28. H. Sun, L. Mei, J. Liang, Z. Zhao, C. Lee, H. Fei, M. Ding, J. Lau, M. Li, C. Wang, *Science*, 356 (2017) 599.
29. C. Lin, C. Niu, X. Xu, K. Li, Z. Cai, Y. Zhang, X. Wang, L. Qu, Y. Xu, L. Mai, *Phys. Chem. Chem.* Phys.18(2016)22146.
30. S. Niu, L. Wei, Z. Chen, Y. Shi, J. Zhao, B. Li, Q.H. Yang, F. Kang, *Journal of Power Sources*, 295 (2015) 182.
31. A. Jing, G. Liang, H. Shi, Y. Yuan, Q. Zhan, W. Feng, *Journal of nanoscience and nanotechnology*, 19 (2019) 7404.
32. S.M. Abbott, J.B. Elder, P. Španěl, D. Smith, *International Journal of Mass Spectrometry*, 228 (2003) 655.
33. C. Zu, A. Manthiram, *Advanced Energy Materials*, 3 (2013) 1008.
34. H.Y. Yue, S. Huang, J. Chang, C. Heo, F. Yao, S. Adhikari, F. Gunes, L.C. Liu, T.H. Lee, E.S. Oh, B. Li, J.J. Zhang, H. Ta Quang, L. Nguyen Van, Y.H. Lee, *Acs Nano*, 8 (2014) 1639.
35. X. Wang, D. Gao, M. Li, H. Li, C. Li, X. Wu, B. Yang, *Scientific Reports*, 7 (2017)7044.

© 2019 The Authors. Published by ESG (www.electrochemsci.org). This article is an open access article distributed under the terms and conditions of the Creative Commons Attribution license (http://creativecommons.org/licenses/by/4.0/).